Pacific Northwest
NATIONAL LABORATORY

PNNL-31418

NRAP-Open-IAM Analytical Reservoir Model

Development and Testing

June 2021

Seunghwan Baek
Diana H Bacon
Nicolas J Huerta

U.S. DEPARTMENT OF ENERGY

Prepared for the U.S. Department of Energy
under Contract DE-AC05-76RL01830

DISCLAIMER

PACIFIC NORTHWEST NATIONAL LABORATORY
operated by
BATTELLE
for the
UNITED STATES DEPARTMENT OF ENERGY
under Contract DE-AC05-76RL01830

Printed in the United States of America

Available to DOE and DOE contractors from the
Office of Scientific and Technical Information,
P.O. Box 62, Oak Ridge, TN 37831-0062;
ph: (865) 576-8401
fax: (865) 576-5728
email: reports@adonis.osti.gov

Available to the public from the National Technical Information Service
5301 Shawnee Rd., Alexandria, VA 22312
ph: (800) 553-NTIS (6847)
email: orders@ntis.gov <https://www.ntis.gov/about>
Online ordering: http://www.ntis.gov

PNNL-31418

NRAP-Open-IAM Analytical Reservoir Model

Development and Testing

June 2021

Seunghwan Baek
Diana H Bacon
Nicolas J Huerta

Prepared for
the U.S. Department of Energy
under Contract DE-AC05-76RL01830

Pacific Northwest National Laboratory
Richland, Washington 99354

Abstract

Geological carbon sequestration (GCS) is a key technology for reducing global carbon dioxide (CO_2) emissions. Over the last decade, the U.S. Department of Energy has invested in understanding the science base, developing practical implementation methods, and demonstrating secure GCS technologies to mitigate the environmental impacts associated with the atmospheric release of CO_2. As part of the National Risk Assessment Partnership, a systems-level risk assessment tool, called the NRAP-Open-IAM, has been developed to conduct risk assessment and enable safe operations at a GCS site. The current NRAP-Open-IAM contains a simple reservoir model component that calculates the evolution of CO_2 saturation and fluid pressure in a storage reservoir during CO_2 injection operations.

This report presents the development and testing of a new analytical reservoir reduced-order model (ROM), which is extended from an existing semi-analytical model for estimation of CO_2 and brine leakage along legacy wells and enhances the capability of the NRAP-Open-IAM to simulate more types of reservoir conditions. The developed model is validated against three reference studies, and the results indicate that the new ROM predicts the behavior of the two-phase fluids (brine and injected CO_2) well and is applicable to different reservoir simulation boundary conditions (i.e., constant pressure boundary and infinite-acting boundary) without *a priori* user specification of the boundary type. Sensitivity analysis for a set of model parameters is performed using 4,000 synthetic cases prepared via a fully automated process and using machine-learning-based feature selection.

The stochastic analysis identifies gravitational number (i.e., ratio of gravitational forces to viscous force) and distance between the injection well and observation location as the most impactful parameters for matching the pressure and CO_2 saturation, respectively, between the numerical simulations and the ROM. This report details the possible ROM uncertainties and serves as a guide for users to understand the use and limitations of this ROM. The code implementation of the model will be released as a module within the NRAP-Open-IAM.

Acknowledgments

This work was completed as part of the U.S. Department of Energy's (DOE's) National Risk Assessment Partnership (NRAP) project, supported by the DOE Office of Fossil Energy's Cross-Cutting Research Program. The work was performed by Pacific Northwest National Laboratory under DOE contract number DE-AC05-76RL01830.

Acronyms and Abbreviations

AoR	area of review
DOE	U.S. Department of Energy
GCS	geological carbon sequestration
MAE	mean absolute error
MI	mutual information
NRAP	National Risk Assessment Partnership
Open-IAM	open source integrated assessment model
ROM	reduced-order model
STOMP	Subsurface Transport Over Multiple Phases

Contents

Figures

Tables

1.0 Introduction

Carbon capture, utilization, and storage technologies are being developed, both domestically and internationally, for their potential to mitigate environmental impacts associated with the atmospheric release of carbon dioxide (CO_2) from anthropogenic sources, such as power generation from fossil fuels and other large industrial sources. Over the last decade, the U.S. Department of Energy (DOE) has invested millions of dollars developing carbon capture technologies and demonstrating safe and secure geologic carbon storage via a number of pilot-scale projects sited throughout the United States (NETL 2015). To date, these projects have stored more than 16 million tonnes of CO_2 (NETL 2018).

Within the U.S., CO_2 injection operations are generally regulated by the U.S. Environmental Protection Agency (EPA) within the Underground Injection Control program through the Class VI regulations promulgated under the Safe Drinking Water Act (USEPA 2010). The Class VI regulations are designed to protect underground sources of drinking water, and include strict requirements for site characterization, construction of CO_2 injection wells, injection operations, site monitoring, financial liability, and recordkeeping/reporting. Key elements of the Class VI permitting process include delineating an area of review (AoR) and defining an appropriate post-injection site care period for the project, both of which require simulating CO_2 saturations and pressure distributions from computational models throughout the project's life. These simulations are based on site-specific data and are updated periodically during the project's lifetime to evaluate reservoir performance and evolution of the storage system.

Despite the sophistication of today's multi-physics reactive transport codes, significant uncertainty exists in predicting the performance of geologic storage reservoirs. Challenges associated with developing greenfield sites include (1) the inherit difficulty in scaling a few point source measurements of geological structure and reservoir permeability derived from characterization of borehole samples throughout the extensive area likely to be impacted by a commercial-scale CO_2 injection; (2) a lack of site-specific data on the geometry of the porous media and resulting transport of the injected CO_2 in the reservoir; and (3) understanding changes in the transport behavior of CO_2 caused by changes in pressure and/or temperature and the buoyant nature of CO_2 over the long time scales required for geologic sequestration to have long-term benefit to atmospheric CO_2 concentration. Additionally, the computational resources required to run high-fidelity simulations limits their usefulness in performing sensitivity analysis for uncertainty reduction.

To help address this need, DOE established the National Risk Assessment Partnership (NRAP), an initiative across five DOE national laboratories with the goal of developing defensible, science-based methodologies and platforms for quantifying risks amidst system uncertainty. In 2017, the NRAP team released a set of 10 tools (i.e., the NRAP Toolset) that can be used to estimate risks associated with geological carbon sequestration (GCS) (NETL 2021a), including the open source integrated assessment model (NRAP-Open-IAM). The NRAP-Open-IAM tool adopts a system-level stochastic approach that includes uncertainties in components (e.g., storage reservoirs, leakage scenarios, and shallow groundwater impacts). The tool is derived from detailed physics and chemistry simulation results that are used to train more computationally efficient models, referred to here as reduced-order models (ROMs), for each component of the system. These tools can be used to help regulators and operators define the AoR and better understand the possible impacts to water quality caused by CO_2 and brine leakage from a storage reservoir into drinking water aquifers to make informed decisions on monitoring and mitigation to reduce risks.

This report details the development and testing of one analytical reservoir model that can be used to (1) predict pressure and CO_2 saturation changes caused by CO_2 injection throughout CO_2 storage reservoirs and (2) feed information to analyze the potential impacts that CO_2 and brine leaking from the storage reservoirs might have on overlying monitoring units (e.g., aquifers). The analytical reservoir model is similar to the existing simple reservoir model within the NRAP-Open-IAM but extends the IAM's capability to simulate additional boundary conditions and two-phase fluid behavior. In this report, the model is presented and validated using three different references for quality assurance. Further, an exhaustive sensitivity analysis is conducted, which allows users to understand the model's capability and limitations and determine its appropriateness for use at their site.

1.1 Analytical Reservoir Model

The fundamental analytical solution was originally developed in Celia et al. (2011) and further modified in the present work to estimate pressure (p_{leak} as in Eq. 16) and CO_2 saturation ($h'(\chi_{leak})$ as in Eq. 7) at an arbitrary distance r at time t for a single injection well in a horizontal, confined, homogeneous deep reservoir or saline aquifer (Figure 1).

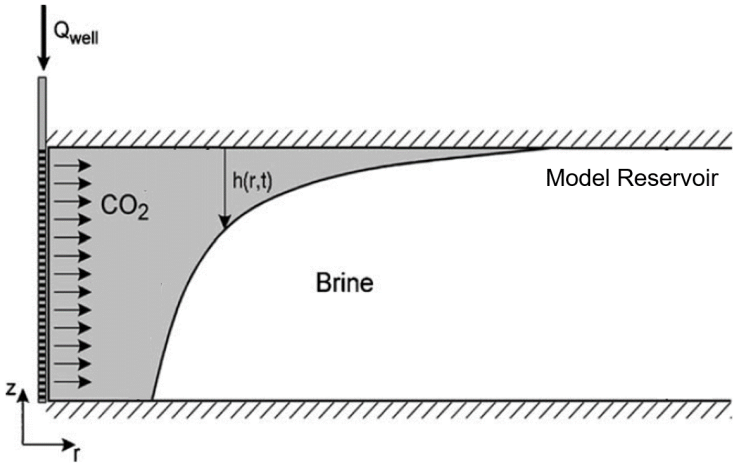

Figure 1. Conceptual schematic of CO_2 plume evolution during CO_2 injection (modified from Celia et al. 2011).

The model was derived with the assumption of strong buoyant segregation, driven by the large density difference between the brine and CO_2. So, once the fluids are separated by the buoyant override of CO_2, they reach vertical equilibrium in their pressure distributions, showing a sharp interface as seen in the gray (CO_2) and white (brine) regions in Figure 1. In the model, there is no vertical communication (i.e., no flow) at the top and bottom of the model, and constant pressure condition is applied at the lateral boundary (i.e., a Dirichlet boundary condition). The details of the model are presented below.

First, relevant dimensionless variables are defined.

$$\Gamma = \frac{2\pi(\rho_B - \rho_C)gkH^2}{\mu_B Q_{well}} = \frac{Gravitational\ force}{Viscous\ force} \quad (1)$$

where Γ gravitational number (-) is a ratio of gravitational force to viscous force, ρ_B is brine density (kg/m^3), ρ_C is CO_2 density (kg/m^3), g is acceleration of gravity (9.8 m/s^2), k is reservoir

permeability (m^2), H is reservoir thickness (m), μ_B is brine viscosity (Pa-sec), Q_{well} is volumetric CO_2 injection rate (m^3/sec).

$$\lambda = \frac{(1 - S_B^{res})\mu_B}{\mu_C} \tag{2}$$

where λ is mobility ratio (-), μ_C is CO_2 viscosity (Pa-sec), S_B^{res} is brine residual saturation (-).

$$\chi_{leak}(t, r_{leak}) = \frac{2\pi H\phi(1 - S_B^{res})r_{leak}^2}{\int Q_{well}\, dt} \tag{3}$$

where χ_{leak} is the relative location of outer boundary of CO_2 plume (-) at time t for given distance r_{leak}, ϕ is porosity (-), r_{leak} is distance from injection well to the leaky well (m), $\int Q_{well}\, dt$ is cumulative CO_2 injection volume (m^3) at a given time.

Next, CO_2 plume thickness, which leads to CO_2 saturation, is calculated differently depending on the value of χ_{leak}. If $\chi_{leak} < {}^{2}/_{\lambda}$

$$h(\chi_{leak}(t, r_{leak})) = (1 - S_B^{res})H \tag{4}$$

where $h(\chi_{leak}(t, r_{leak}))$ is CO_2 plume thickness at time t.

Else if $\chi_{leak} > 2\lambda$

$$h(\chi_{leak}(t, r_{leak})) = 0 \tag{5}$$

else

$$h(\chi_{leak}(t, r_{leak})) = \frac{1}{\lambda - 1}\left(\sqrt{\frac{2\lambda}{\chi_{leak}}} - 1\right)H \tag{6}$$

$$h'(\chi_{leak}(t, r_{leak})) = \min\left(h(\chi_{leak}(t, r_{leak})), 1 - S_B^{res}\right) \tag{7}$$

where $h'(\chi_{leak})$ is the vertically averaged CO_2 saturation at time t and at the leaky well location, r_{leak}.

According to whether the pressure propagation caused by CO_2 injection reaches the boundary of the reservoir, the dimensionless variable for the location of the pressure front is determined differently.

$$\psi_{infinite} = \frac{4.5\pi H\phi k(1 - S_B^{res})}{\mu_B c_{eff} Q_{well}} \tag{8}$$

where $\Psi_{infinite}$ is the location of the outer boundary of pressure front at which the pressure has not changed relative to the initial pressure, c_{eff} is the brine compressibility (1/Pa).

$$\psi_{finite} = \frac{2\pi H\phi(1 - S_B^{res})r_{res}^2}{\int Q_{well}\, dt} \tag{9}$$

where Ψ_{finite} is the location of the outer boundary of pressure front at which the pressure has changed relative to the initial pressure, and r_{res} is the distance from the injection well to reservoir boundary (m).

$$\psi = \min\left(\psi_{infinite}, \psi_{finite}\right) \tag{10}$$

This approach allows to handle both constant pressure boundary condition and infinite-acting flow reservoir boundary condition without specification as input setting.

$$F(h'(\chi_{leak})) = \frac{-\lambda}{\lambda - 1}\left(h'(\chi_{leak}) + \frac{\ln[(\lambda - 1)\cdot h'(\chi_{leak}) + 1]}{\lambda - 1}\right) \tag{11}$$

where F is a pressure offset (Pa) associated with the vertical pressure distribution.

If $\chi_{leak} \geq \psi$

$$\Delta p'(\chi_{leak}) = 0 \tag{12}$$

where $\Delta P'(\chi_{leak})$ is the change in pressure (Pa) relative to the initial value.

Else if $\psi > \chi_{leak} > 2\lambda$

$$\Delta p'(\chi_{leak}) = -\frac{1}{2\Gamma}\ln\left(\frac{\chi_{leak}}{\psi}\right) + F(h') \tag{13}$$

else if $2\lambda > \chi_{leak} > {}^{2}/_{\lambda}$

$$\Delta p'(\chi_{leak}) = \frac{1}{\Gamma} - \frac{1}{\Gamma}\sqrt{\frac{\chi_{leak}}{2\lambda}} - \frac{1}{2\Gamma}\ln\left(\frac{2\lambda}{\psi}\right) + F(h') \tag{14}$$

else ${}^{2}/_{\lambda} > \chi_{leak}$

$$\Delta p'(\chi_{leak}) = -\frac{1}{2\lambda\Gamma}\ln\left(\frac{\chi_{leak}\lambda}{2}\right) + \frac{1}{\Gamma} - \frac{1}{\Gamma\lambda} - \frac{1}{2\Gamma}\ln\left(\frac{2\lambda}{\psi}\right) + F(h') \tag{15}$$

$$p_{leak}(t) - p_{ini} = \max\left(0, \Delta p'(\chi_{leak})\cdot(\rho_B - \rho_C)gH\cdot p_{grad}\right)$$

$$p_{leak}(t) = p_{ini} + \max\left(0, \Delta p'(\chi_{leak})\cdot(\rho_B - \rho_C)gH\cdot p_{grad}\right) \tag{16}$$

where $p_{leak}(t)$ is the vertically averaged pressure (Pa) at the leaky well location at time t, p_{ini} is the initial reservoir pressure (Pa), p_{grad} is the pressure gradient (Pa/m).

2.0 Methodology

This section describes the benchmark problem introduced in Ebigbo et al. (2007), parameter sampling, and numerical simulations for validation and sensitivity analysis of the developed analytical ROM. For the validation, three different references are used: 1) Princeton web simulator – an analytical calculation simulator developed by Princeton University Subsurface Hydrology Research Group, 2) STOMP (Subsurface Transport Over Multiple Phases Simulator) – a multi-phase flow simulator developed by Pacific Northwest National Laboratory (White et al. 2012), and 3) Eclipse 100 – a black oil multi-phase flow simulator (Schlumberger n.d.). For the sensitivity analysis, Eclipse 100 is used.

2.1 Benchmark Problem

For model validation, one popular benchmark problem for CO_2 leakage (Ebigbo et al. 2007) is adopted in this study. This problem consists of a 2D reservoir with one injection well and one leaky well and is shown in map view on Figure 2. The leaky well (observation well) is located 100 m away from the injection well. The problem assumes that fluid properties such as density and viscosity are constant, all processes are isothermal, and mutual dissolution between CO_2 and brine is neglected. The Dirichlet boundary conditions (constant pressure) are used for lateral boundaries, and no flow is considered vertically. The model formation is isotropic and capillary pressure is negligible. The simulation parameters are summarized in Table 1. Based on this model problem, three different simulators were used (i.e., Princeton web simulator, STOMP, and Eclipse 100).

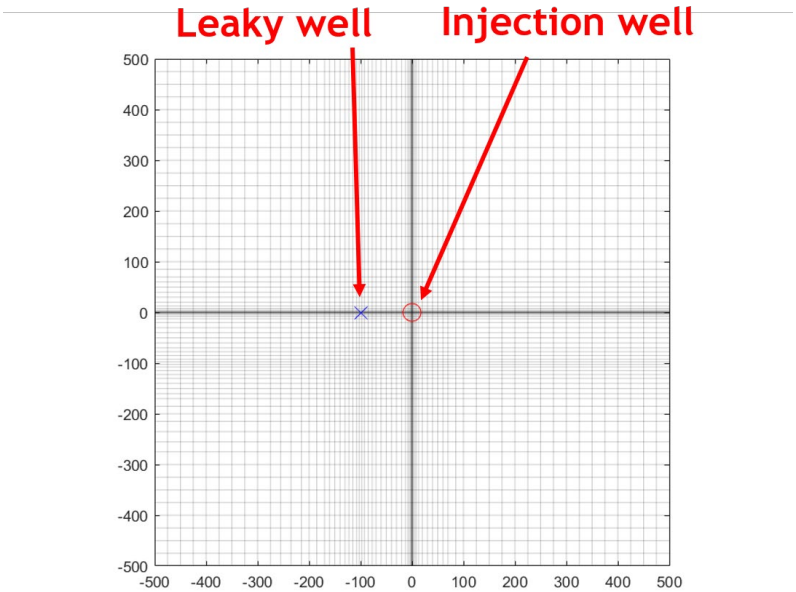

Figure 2. Top view of the mesh and well locations for the benchmark problem used to validate our model.

Table 1. Simulation parameters for the benchmark problem.

Parameter	Units	Value
CO_2 density	kg/m^3	479
Brine density	kg/m^3	1,045
CO_2 viscosity	Pa-sec	3.95×10^{-5}
Brine viscosity	Pa-sec	2.54×10^{-4}
Reservoir permeability	m^2	2.0×10^{-14}
Reservoir thickness	m	30
Porosity	-	0.15
Mass injection rate	kg/s	8.87
Distance between wells	m	100
Dimensions of model domain	m	1,000 × 1,000 × 30
Simulation time	days	1,000

2.2 Case Generation for the Sensitivity Analysis

In addition to the benchmark problem, the developed model was analyzed for wider ranges of conditions. A sensitivity analysis was conducted by comparing the analytical solution with full physics numerical simulation using Eclipse 100 (Schlumberger. n.d.) to determine which parameters impact errors in CO_2 saturation and pressure. To generate simulation models for realistic conditions, the ranges of geological parameters (Figure 3) were set to cover the values used in studies that have been conducted for various GCS sites in the U.S. (Appendix A).

Geological Parameters	Unit	Ranges	
		Min	Max
Permeability	m^2	0.5×10^{-15}	1.0×10^{-12}
Porosity	-	0.10	0.3
Lateral size[a]	km	5	100
Thickness	meter	15	500
Bottom depth	meter	850	4,000
Pressure gradient	MPa/km	9.80	14.7
Temperature gradient	°C/km	15	30
Salt mass fraction	-	0.001	0.25
Brine residual sat	-	0.001	0.20
Period	Year	5	50
Total injection amount	MT	1	250
Distance ratio to observation well[a]	-	0.2	0.8

Model Parameters	Unit	Ranges	
		Min	Max
Initial pressure	MPa	8.6	58.2
Brine density	kg/m^3	965.3	1,194.8
Brine viscosity	Pa-sec	2.36×10^{-4}	15.88×10^{-4}
Brine compressibility	1/Pa	3.63×10^{-12}	2.31×10^{-11}
Injection rate[b]	kg/sec	1.1	1,496.5
Distance from the Injection well	meter	500	40,000
CO_2 density	kg/m^3	598.5	976.0
CO_2 viscosity	Pa-sec	0.455×10^{-4}	1.043×10^{-4}

Figure 3. Ranges of geologic parameters used to generate 4,000 unique combinations using Latin hypercube sampling, and relationship (colored arrows) to model parameters which are calculated based on the geological parameters and relevant correlations. [a] Discrete values are sampled. [b] This range is 0.033 to 47.20 MT/yr.

A total of 4,000 cases were generated with a near-random combination of the parameters based on Figure 3 and Latin hypercube sampling (Iman et al. 1981). The model parameters, which are directly used for both numerical and analytical calculations, were calculated from the geological parameters with relevant correlations and constitutive models linking independent to dependent variables. For the calculation of the fluid properties (e.g., brine density, brine viscosity, CO_2 density, and CO_2 viscosity), the same methods to that of STOMP were used (White at al. 2012).

2.3 Numerical Simulation

For the sensitivity analysis, the automation of the numerical simulation with varying parameters is required. In this study, Eclipse 100 was used to generate the full physics simulations, followed by comparison with the results of the analytical ROM. The input file is generated for each case based on the parameters set above. The generation of the input file and its sequential execution were fully automated with a custom MATLAB script.

A 3D homogeneous reservoir is modeled in the numerical simulation. In each model, there are two wells total: one for injection and one for observation. The injection well is located at the center of the model domain, while the location of the observation well varies with lateral dimension and distance ratio set differently in each case. (Figure 3 shows four examples of this ratio.) In the study, 5, 10, 25, 50 and 100 km in the lateral dimension and 0.2, 0.4, 0.6 and 0.8 of

the distance ratios were used respectively. For grids of the simulation, the predefined meshes were prepared with Abaqus (Dassault Systems. n.d.) and used. For speed and stability of the numerical simulation, tartan grids were used, and were focused (i.e., highly discretized) around the injection and observation wells (Figure 4). The automated process of input file generation first reads the lateral dimension and distance ratio of the distance between boundary and observation well and distance between injection well and observation well and then loads the corresponding mesh information from the predefined mesh files into the input file. Constant pressure boundary condition (i.e., a Dirichlet boundary condition) was adopted for lateral boundaries by setting the pore volume multiplier values to be large (i.e., 1×10^7) for the boundary cells. The diameter of the well is 0.00127 m for all cases, and the well is perforated through all cells at the center across the formation.

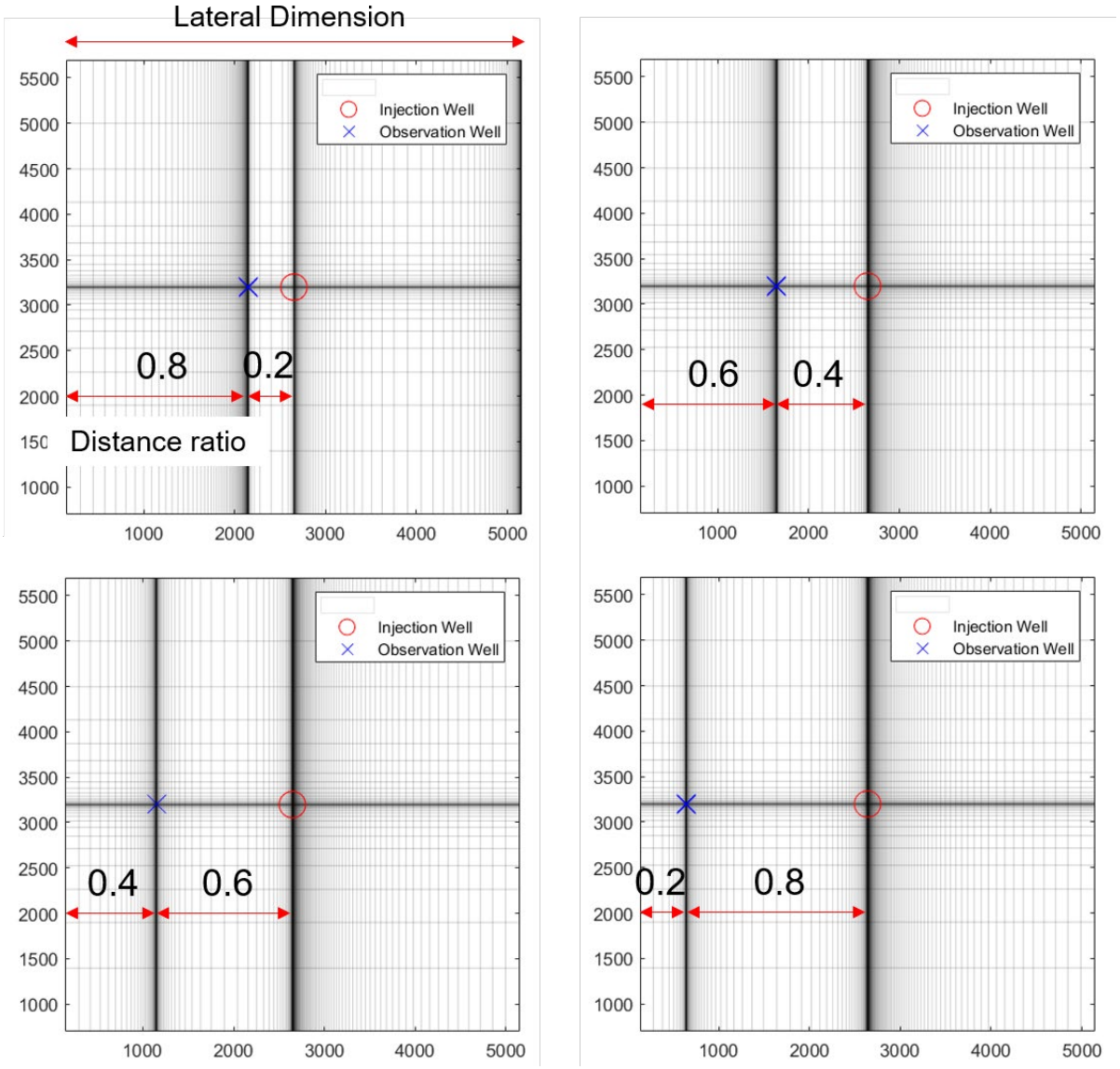

Figure 4. Top view of the grids used for numerical simulation. 3D homogeneous reservoir is modeled. The injection well is at the center of the reservoir. For each case, the lateral dimension sizes, the location of the observation well, and distance ratio vary. The unit of dimension size is meters.

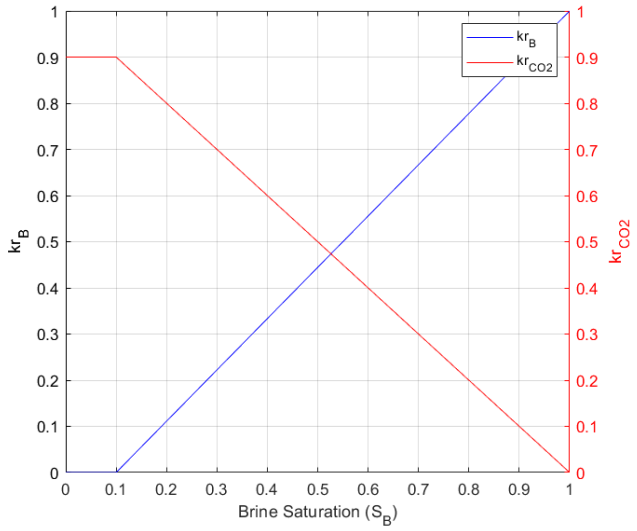

Figure 5. An example of relative permeability curves implemented in the numerical simulations. Relative brine permeability (kr_B) and relative CO_2 permeability (kr_{CO2}) are plotted as a function of brine saturation(S_B). The residual water saturation (S_B^{res}) is 0.1.

The model reservoir is initially saturated with only brine ($S_B = 1$), and its residual brine saturation (S_B^{res}) varies over cases between 0.001 and 0.20. For multiphase fluid flow, linear relative permeability curves were used (Figure 5). Accordingly, for numerical simulations, a different relative permeability lookup table was constructed with different residual brine saturation values for each case. The brine and CO_2 fluid density and viscosity were calculated based on initial average pressure and temperature (i.e., values at the middle of the model reservoir in a vertical direction), which are dependent on formation depth, thickness, pressure gradient, and temperature gradient. No changes in density and viscosity associated with CO_2 injection were considered. Capillary pressure was set to zero, and rock pore volume was considered incompressible. Gravity effect was considered.

2.4 Data Filtering

All parameters considered in the present work (Figure 3) are collected from literature and chosen within physically feasible ranges. However, the arbitrary combination of many parameters can lead to unacceptable operational conditions (e.g., an injection pressure above the maximum allowable CO_2 injection pressure), and in such cases, an *a posteriori* data filtering approach is used.

Regarding CO_2 injection pressure change, under the Underground Injection Control Program for Carbon Dioxide Geologic Sequestration Wells (USEPA 2010), referred to as the Class VI Rule, the U.S. Environmental Protection Agency requires that the injection pressure not exceed 90% of the fracture pressure in the injection zone to ensure that CO_2 injection does not initiate new fractures or propagate existing ones (40 CFR 146.88(a)) (Appriou 2019). Thus, the estimation of the fracture pressure is critical. However, fracture pressure is site-specific and is difficult to generalize. In the present study, the cases showing pressure increases two times higher than the absolute in-place hydrostatic pressure were removed. As a result, only 3,619 cases out of the total 4,000 cases were considered for further analysis. Fracture pressure gradient is between hydrostatic pressure gradient and overburden pressure gradient, and the general

assumption for the overburden pressure gradient (22.62 MPa/km = 1 psi/ft) is around 2.3 times of the hydrostatic pressure gradient (9.8 MPa/km = 0.44 psi/ft) (Eaton 1969). So, although allowing a pressure increase of up to two times the hydrostatic pressure can be considered optimistic, the analytical solution has freedom to be tested outside of the acceptable limitations, and users need to be cautious about the validity of the model input values.

2.5 Error Calculation

To analyze the accuracy of pressure and saturation predictions for the analytical solution, when compared to the numerical calculation, mean absolute error (MAE) [Eq. (17)] and relative percent error [Eq. (18))] were employed to quantify the error of the time-series pressure and saturation data respectively for each case.

$$Mean\ absolute\ error\ (MAE) = \frac{\sum_{i=1}^{n_T}\left|P_{i,anal}\ (or\ S_{CO2,i,anal}) - P_{i,ref}\ (or\ S_{CO2,i,ref})\right|}{n_T} \quad (17)$$

$$Relative\ error, \% = \frac{\left|P_{i,anal}\ (or\ S_{CO2,i,anal}) - P_{i,ref}\ (or\ S_{CO2,i,ref})\right|}{P_{i,ref}\ (or\ S_{CO2,i,ref})} \times 100 \quad (18)$$

$P_{i,anal}$ is vertically averaged pressure predicted by the analytical solution at the observation location at the timestep i, while $P_{i,ref}$ is a reference value calculated by Eclipse 100. n_T is the total number of the timesteps. MAE and relative errors for CO_2 saturation were calculated in the same manner.

2.6 Sensitivity Analysis

Mutual information (MI) (Cover and Thomas 1991; Shannon and Weaver 1949) was used to analyze the impacts of associated parameters [Eq. (1) to Eq. (16)] on prediction accuracy of the analytical solution. MI is a measure of the mutual dependence between two variables. It is a dimensionless quantity and can be regarded as the reduction in uncertainty about one variable given knowledge of another. The value of MI is inversely proportional to the uncertainty, and thus zero MI indicates the two variables are independent. MI between the model input parameters or coupled parameters such as gravitational number (Γ) and MAE of each case was calculated for pressure and CO_2 saturation, respectively. In addition, the concept of impurity-based feature importance was applied to quantify the sensitivity of individual parameter with two different machine learning algorithms: decision tree (Breiman et al. 1984) and random forest (Breiman 2001). With each algorithm, the importance of one parameter is computed as the total reduction of the criterion brought by the parameter. *Scikit-learn library* (Pedregosa et al. 2011) was used for both MI and the impurity-based feature importance calculations.

3.0 Results & Discussion

This section discusses the results of the validation and sensitivity analysis. Following the validation with the numerical simulation results, the predictive capability of the ROM and the impact of the associated parameters are investigated.

3.1 Analytical ROM Validation

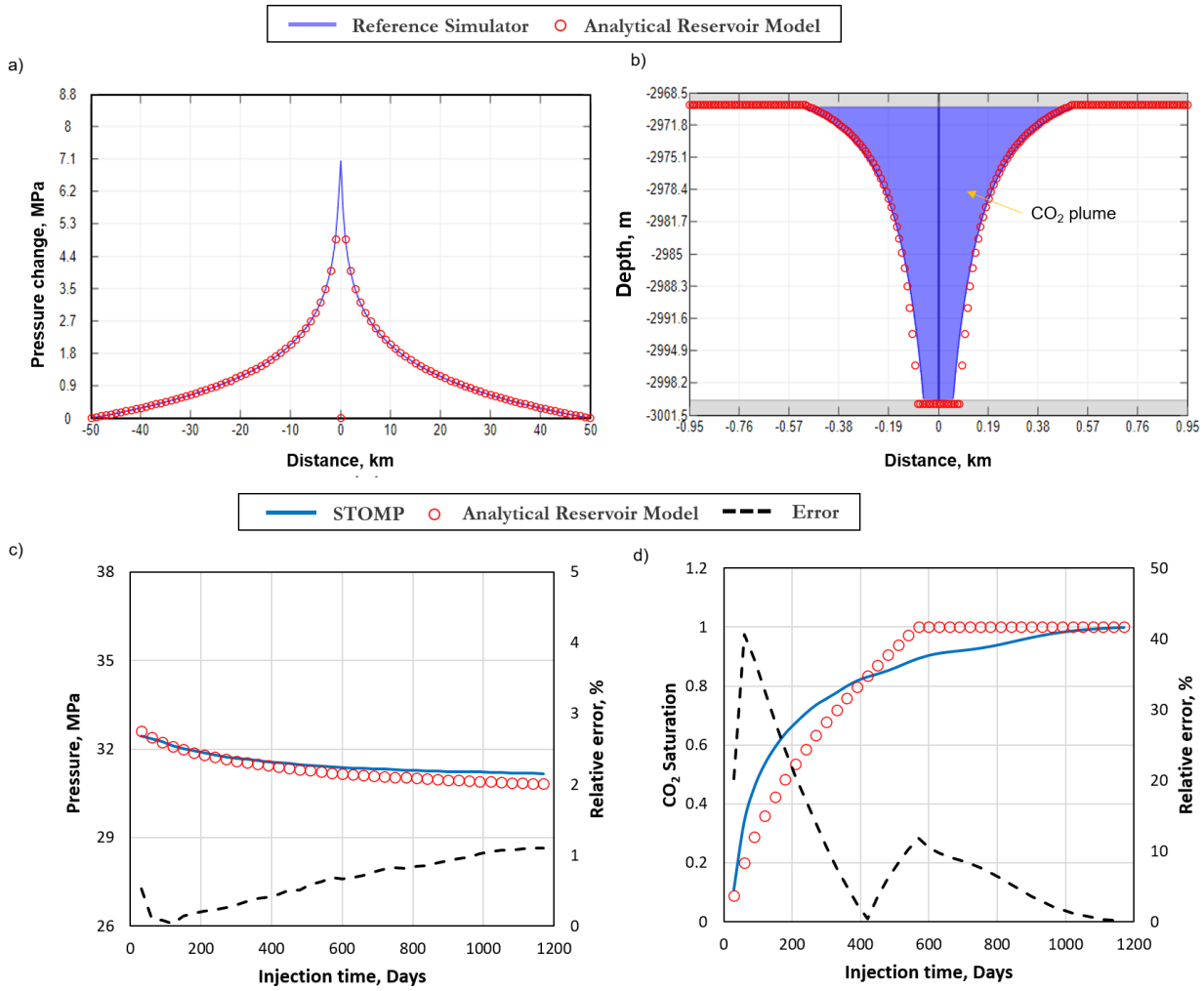

Figure 6. Model validation with the benchmark problem. Comparison with the Princeton web simulator at 1 year of CO_2 production for a) pressure and b) CO_2 plume evolution in blue. Comparison with STOMP at the observation well location for c) pressure and d) CO_2 saturation.

The Subsurface Hydrology Research Group at Princeton University provides a web-based simulator, which is built based on the work by Celia et al. (2011) (Princeton University Subsurface Hydrology Research Group n.d.). Our analytical model is validated against the Princeton web simulator and STOMP (White et al. 2012) based on the benchmark problem (Ebigbo et al. 2007). For the comparison with the web simulator, 100 km of the reservoir's later

boundary size was tested instead of 1 km. In Figure 6a and Figure 6b, pressure and CO_2 plume profiles (blue line) are compared at 1 year of CO_2 injection, which shows good agreement to the Princeton web simulator (red circles). Also, Figure 6c and Figure 6d show that the analytical model predicts well the results of the numerical calculation of STOMP over time. The pressure and CO_2 saturation are vertically averaged values at the observation well location.

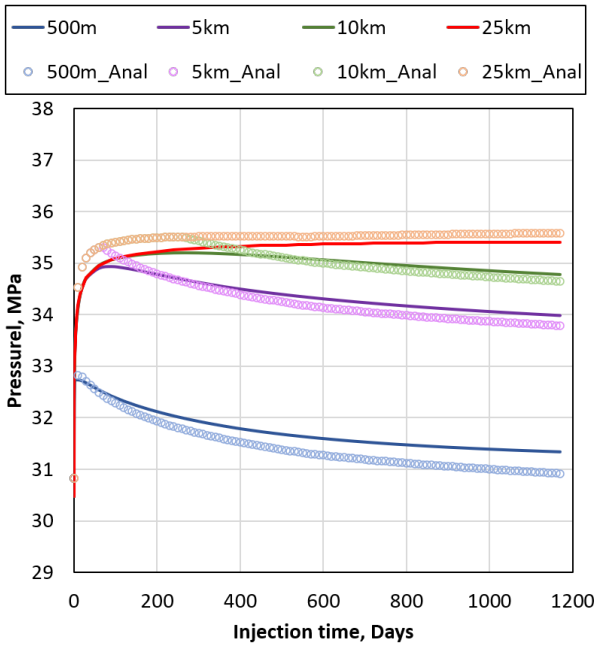

Figure 7. Validation for different reservoir boundary sizes. Solid lines and open circles are calculated with Eclipse 100 and the analytical solution, respectively.

Further validation was performed for different boundary sizes of the reservoir – 1, 10, 20, and 50 km. Except for the boundary size, all parameters were kept the same as in Table 1. Figure 7 shows that the analytical solution matches well the numerical results regardless of the boundary sizes. The pressure reduction is observed for 1, 10, and 20 km, which is a result of the constant pressure boundary condition applied. No pressure reduction, in contrast, is observed in the case of 50 km. This is because pressure does not reach the boundary, and thus it can be considered an infinite-acting reservoir. The good matching indicates that the developed analytical model can be applicable to both constant pressure and infinite boundary conditions.

3.2 Parameter Sensitivity – Pressure

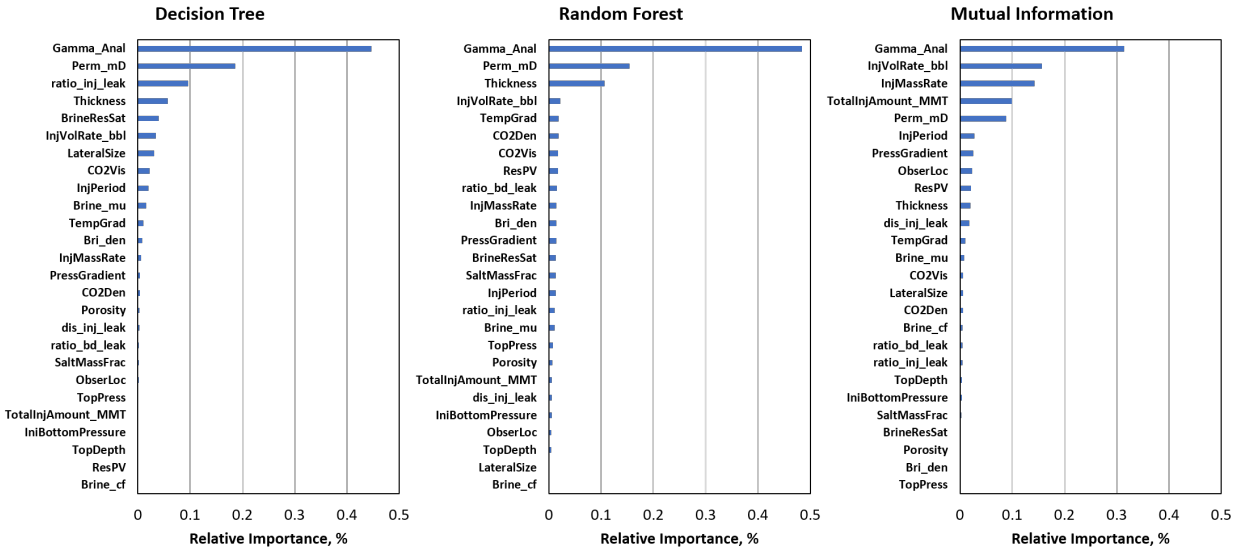

Figure 8. Sensitivity analysis for pressure. The relative importance (impacts) to the model accuracy is quantified. *Gamma_Anal*, gravitational number, is ranked top in three different analyses.

The importance of each parameter to the model accuracy was analyzed on the basis of the impurity-based feature importance and MI. Figure 8 shows the relative importance, in descending order for key parameters, to accurately predicting pressure using the analytical model [Eq. (1) to Eq. (17)] as identified using three different statistical approaches. As expected, the gravitational number is the most impactful to the accuracy of the developed model.

The gravitational number and MAE are plotted for 3,619 cases at log-log scale in Figure 9a. The clear dependency of the MAE on the gravitational number is observed, and a higher gravitational number results in a higher accuracy with the developed analytical approach. Physically, as described in Eq. (1), the dimensionless gravitational number indicates the ratio of the gravitational force to viscous force. With a high gravitational number (Figure 9b), the stronger gravitational forces drive a distinct gravity-driven segregation of the in-place brine and injected CO_2. In contrast, with a low gravitational number, the stronger viscous forces lead to a more cylindrical plume shape (Figure 9c). The original analytical solution was mathematically derived with the assumption of a distinct buoyant override and segregation of the fluids as seen in Figure 9b.

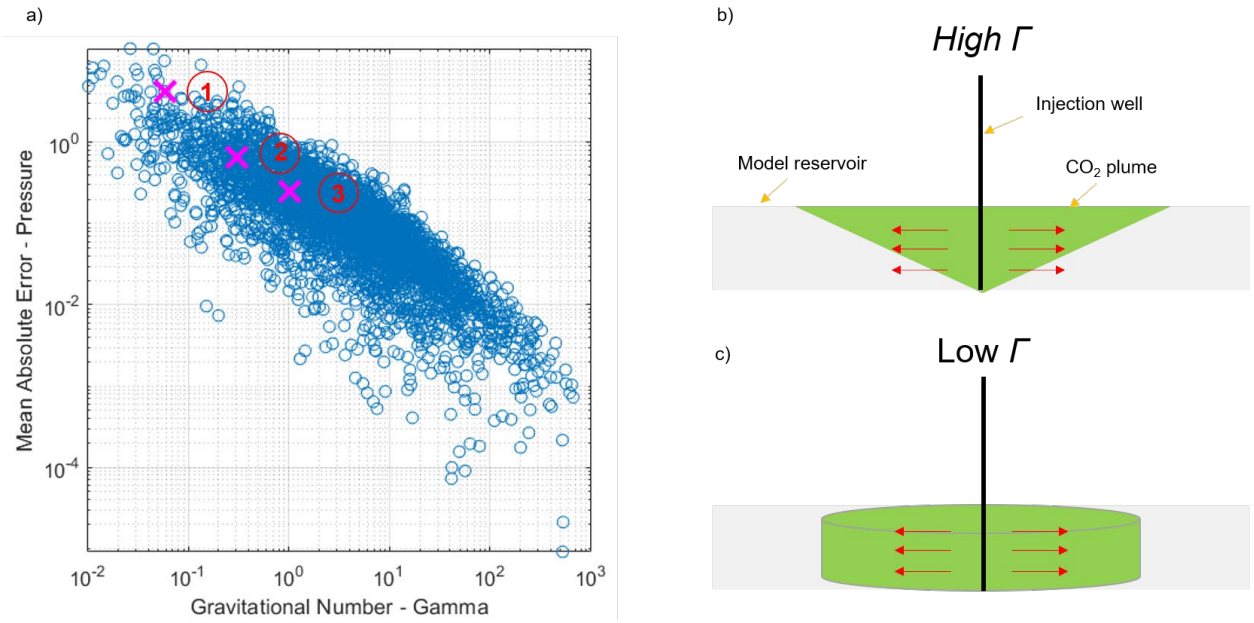

Figure 9. Impacts of the gravitational number: a) the dependency of mean absolute error of pressure on gravitational number, b) plume evolution with high gravitational number, c) plume evolution with low gravitational number.

3.3 Case Study – Pressure

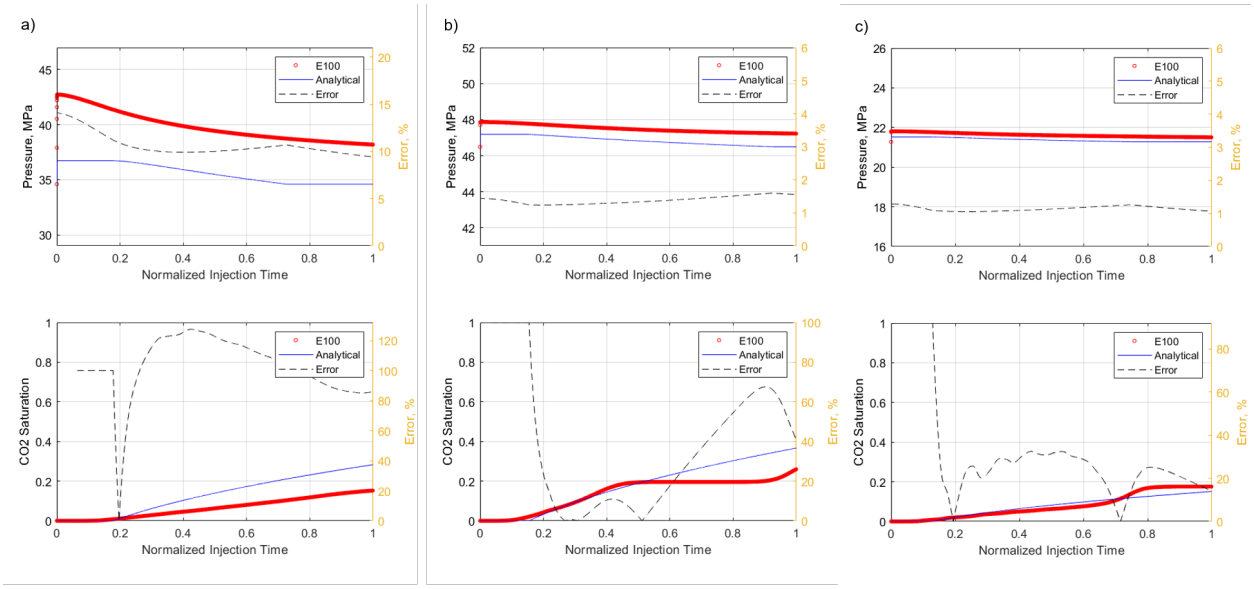

Figure 10. Pressure history comparison: a), b), and c) correspond to the cases 1, 2, and 3 in Figure 9a. Top row: pressure. Bottom row: CO_2 saturation. The x-axis is normalized injection time, and the secondary axis is relative error. For numerical calculation, Eclipse 100 was used (E100).

Time-series pressure and CO_2 saturation data are compared in Figure 10 for three cases marked in Figure 9a (magenta X's) to provide a better sense of the degree of MAE over time. The top row of panels in Figure 10 shows the pressure comparison, and the saturation histories are given on the bottom row for completeness. The injection period varies by realization case, so it is normalized to the total injection interval. MAEs for pressure (Γ) are 4.248 (0.0583), 0.657 (0.3020) and 0.017 MPa (1.0163) for Figure 10a, Figure 10b, and Figure 10c, respectively. It clearly shows that the overall error reduces with increasing gravitational number (left to right). Note that the pressure difference is distinct in Figure 10a although the relative error is less than 15%. The larger relative error is observed for CO_2 saturation, and this is because of the scale of the saturation.

3.4 Parameter Sensitivity – CO_2 Saturation

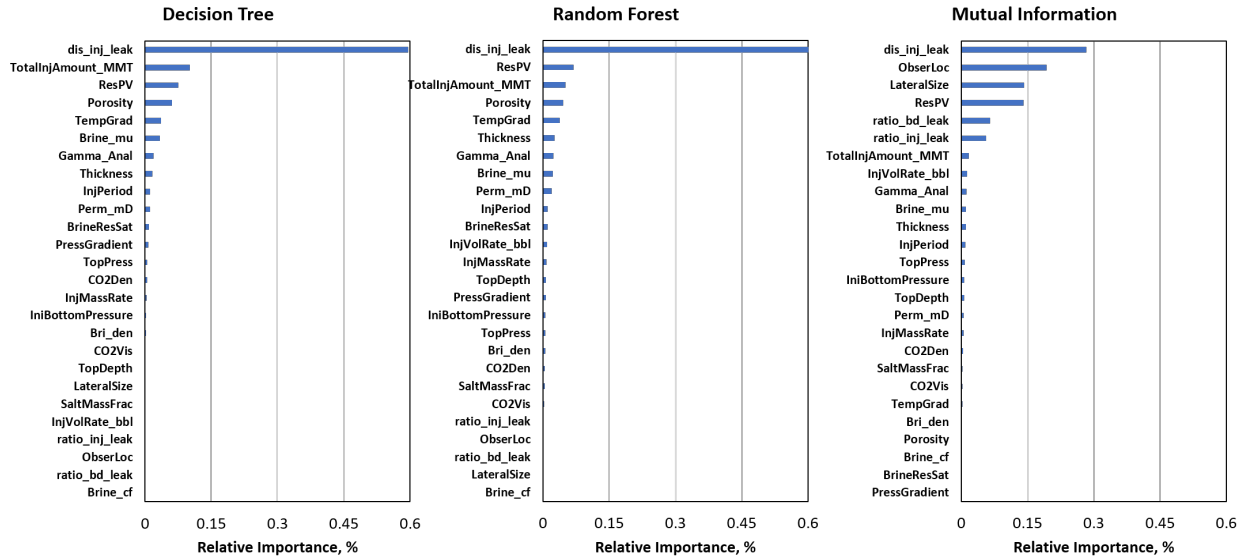

Figure 11. Sensitivity analysis for CO_2 saturation. The relative importance (i.e., impacts) to the model accuracy is quantified. The distance between injection well and observation location, denoted as *dis_inj_leak*, is ranked top in three different analysis.

The importance of each parameter to model accuracy for CO_2 saturation was analyzed in the same manner. Figure 11 shows the relative importance to saturation prediction accuracy of the analytical model [Eq. (1) to (16)] in descending order, and three different statistical approaches show that the distance between injection well and observation location, denoted as *dis_inj_leak*, is the most impactful to the accuracy of the developed model.

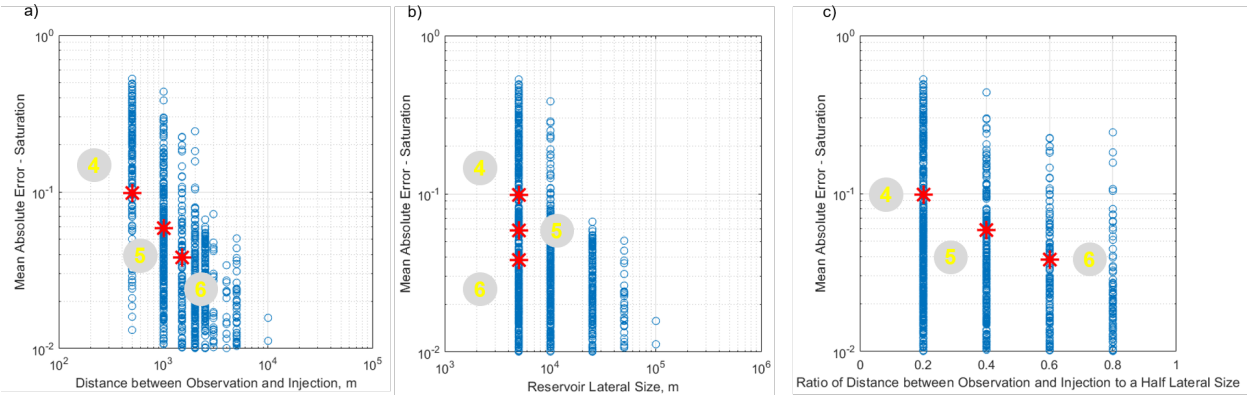

Figure 12. Impacts of the observation location: a) the dependency of mean absolute error of CO_2 saturation on distance between observation and injection well, b) reservoir lateral size, c) distance ratio of the distance between observation and injection well to the distance between reservoir boundary and injection well.

Figure 12 shows the impacts of the observation location. In the case of CO_2 saturation, MAE is relatively small compared to that of pressure, and here only a portion of the 3,619 cases are shown, omitting cases with MAEs below 0.01. The clear dependency of the MAE on the distance between observation and injection well is observed in Figure 12a, and the longer distance results in less error between the analytical model and the numerical simulations. Figure 12b and Figure 12c support the hypothesis that the relative position of the observation well against the injection well and boundary is important for model accuracy. The larger a reservoir's lateral size is, and the farther away the observation location is from the injection well, the smaller the MAE is for CO_2 saturation. Also, a relatively shorter distance between the observation and injection compared to the distance between the observation and domain boundary causes a larger MAE.

3.5 Case Study – CO_2 Saturation

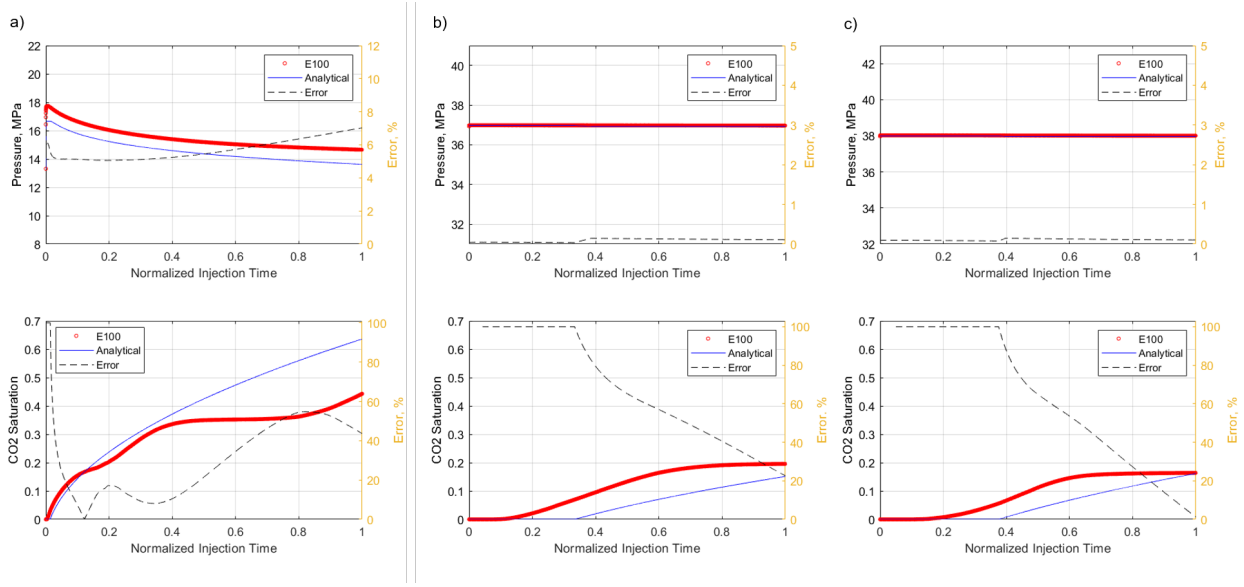

Figure 13. Saturation history comparisons: a), b), and c) correspond to the cases 4, 5, and 6 in Figure 12. Top row: pressure. Bottom row: CO_2 saturation. The x-axis is normalized injection time, and the secondary axis is relative error. For numerical calculation, Eclipse 100 was used (E100).

Time-series data is compared in Figure 13 for three cases identified in Figure 12. The figure panels in the top row show the pressure histories at the observation locations and the figure panels in the bottom row show CO_2 saturation for the corresponding cases at the observation location. The normalized injection period is used for case comparison. MAEs for saturation (distance between the injection and observation wells) are 0.0981 (500 m), 0.0588 (1,000 m), and 0.0381 (1,500 m) for Figure 13a, Figure 13b and Figure 13c, respectively. The MAE is relatively smaller than that of pressure because the scale of the saturation is smaller, while the relative error is larger. The comparison in Figure 13 shows that the overall error reduces with increasing distance between the injection and observation wells (left to right).

4.0 Conclusion

The present work introduces the development and testing of a new analytical reservoir ROM that can be used to estimate CO_2 saturation and pressure changes caused by CO_2 injection throughout a CO_2 storage reservoir and, when incorporated into the NRAP-Open-IAM, can be used to feed data to analyze the potential impacts that CO_2 and brine leaking from the storage reservoirs might have on overlying aquifers or monitoring units for GCS applications. The original model in Celia et al. (2011) is elaborated on for code implementation and to improve its capabilities for different boundary conditions and over-pressured formations.

Validation is performed via three approaches: 1) comparison with the Princeton web simulator (Princeton University Subsurface Hydrology Research Group n.d.), which was developed by the authors of the original model; 2) comparison with full-physics simulator STOMP (White et al. 2012) based on the popular benchmark problem (Ebigbo et al. 2007); and 3) use of machine learning and stochastic realizations of a full physics simulator, Eclipse 100 (Schlumberger. n.d.), to inform the accuracy and sensitivity of the new model over a range of geologically relevant conditions.

This process demonstrates that the prediction accuracy of this new model is quite high given its reduced-order nature and it can be used for different boundary conditions (i.e., constant pressure boundary and infinite-acting reservoir boundary) without *a priori* user specification. The sensitivity analysis conducted with machine learning further shows that gravitational number and distance between the injection well and observation location play a critical role in the model accuracy for pressure and CO_2 saturation, respectively. From a practical perspective, when gravitational number is low and viscous forces dominate gravitational forces, there is a resulting larger error in pressure estimation, which is in line with the model's assumptions of a strong buoyant segregation of fluids. Additionally, since error is reduced when the domain size is large, a user should pick a sufficiently large reservoir to avoid any boundary effects. These insights are useful when a user employs this new reservoir model in the larger NRAP-Open-IAM.

Finally, this report provides readers with case studies and results that enable estimation of potential uncertainties in their site-specific studies. This model is subject to further improvements as the NRAP codes evolve to meet user needs, and the code implementation will be released as part of the NRAP-Open-IAM (NETL 2021b).

5.0 References

40 CFR 146.88(a). *Injection well operating requirements*. U.S. Code of Federal Regulations.

Appriou D. 2019. *Assessment of the Geomechanical Risks Associated with CO_2 Injection at the FutureGen 2.0 Site. Application of the State of Stress Assessment Tool (SOSAT)*. PNNL-28657, Pacific Northwest National Laboratory, Richland, WA.

Akinnikawe O and CA Ehlig-Economides. 2016. "Geologic model and fluid flow simulation of Woodbine aquifer CO_2 sequestration." *International Journal of Greenhouse Gas Control* 49(June):1-13. https://doi.org/10.1016/j.ijggc.2016.02.014

Breiman L. 2001. "Random Forests." *Machine Learning* 45(October):5-32. https://doi.org/10.1023/A:1010933404324

Breiman L, J Friedman, CJ Stone, and RA Olshen. 1984. *Classification and Regression Trees.* Thomson Wadsworth, Belmont, CA.

Birkholzer JT and Z Quanlin. 2009. "Basin-scale hydrogeologic impacts of CO_2 storage: Capacity and regulatory implications." *International Journal of Greenhouse Gas Control* 3(December):745-756. https://doi.org/10.1016/j.ijggc.2009.07.002

Bacon DH, DI Demirkanli, and SK White. 2020. "Probabilistic risk-based Area of Review (AoR) determination for a deep-saline carbon storage site." *International Journal of Greenhouse Gas Control* 102(November):103153. https://doi.org/10.1016/j.ijggc.2020.103153

Cover TM and JA Thomas. 1991. *Elements of Information Theory*. John Wiley & Sons, New York, NY.

Celia MA JM Nordbotten, B Court, M Dobossy, and S Bachu. 2011. "Field-scale application of a semi-analytical model for estimation of CO_2 and brine leakage along old wells." *International Journal of Greenhouse Gas Control* 5(March):257-269. https://doi.org/10.1016/j.ijggc.2010.10.005

Cumming L, J Hawkins, J Sminchak, M Valluri, and N Gupta. 2019. "Researching candidate sites for a carbon storage complex in the Central Appalachian Basin, USA." *International Journal of Greenhouse Gas Control* 88(September):168-181. https://doi.org/10.1016/j.ijggc.2019.05.030

Doughty C. 2009. "Investigation of CO_2 Plume Behavior for a Large-Scale Pilot Test of Geologic Carbon Storage in a Saline Formation." *Transport in Porous Media* 82(May):49-76. https://doi.org/10.1007/s11242-009-9396-z

Dassault Systems. n.d. "ABAQUS/STANDARD." Accessed May 7, 2021. https://www.3ds.com/products-services/simulia/products/abaqus/abaqusstandard

Ebigbo A, H Class, and R Helmig. 2007. "CO_2 leakage through an abandoned well: problem-oriented benchmarks." *Computers & Geosciences* 11(December):103-115. https://doi.org/10.1007/s10596-006-9033-7

Eaton BA. 1969. “Fracture Gradient Prediction and Its Application in Oilfield Operations.” *Journal of Petroleum Technology* 21(October):1353-1360. https://doi.org/10.2118/2163-PA

Finley RJ. 2014. “An overview of the Illinois Basin – Decatur Project.” *Greenhouse Gases: Science and Technology* 4(September):571-579. https://doi.org/10.1002/ghg.1433

Iman RL, JC Helton, and JE Campbell. 1981. “An Approach to Sensitivity Analysis of Computer Models: Part I—Introduction, Input Variable Selection and Preliminary Variable Assessment.” *Journal of Quality Technology* 13(3):174-183. https://doi.org/10.1080/00224065.1981.11978748

NETL. 2015. *Carbon Storage Atlas*, 5th edition. Pittsburgh, PA.

NETL. 2018. Carbon Storage Research. Accessed May 7, 2021. https://netl.doe.gov/coal/carbon-storage/publications

NETL. 2021a. National Risk Assessment Partnership. Accessed May 26, 2021. https://edx.netl.doe.gov/nrap

NETL. 2021b. NRAP-Open-IAM. Accessed May 26, 2021. https://gitlab.com/NRAP/OpenIAM

Nguyen BN, Z Hou, DH Bacon, GV Last, and MD White. 2017. “Analysis of a complex faulted CO_2 reservoir using a three-dimensional hydro-geochemical-mechanical approach.” *Energy Procedia* 114(July):3496-3506. https://doi.org/10.1016/j.egypro.2017.03.1479

Onishi T, MC Nguyen, JW Carey, B Will, W Zaluski, DW Bowen, BC Devault, A Duguid, Q Zhou, SH Fairweather et al. 2019. “Potential CO_2 and brine leakage through wellbore pathways for geologic CO_2 sequestration using the National Risk Assessment Partnership tools: Application to the Big Sky Regional Partnership.” *International Journal of Greenhouse Gas Control* 81(February):44-65. https://doi.org/10.1016/j.ijggc.2018.12.002

Pedregosa F, G Varoquaux, A Gramfort, V Michel, B Thirion, O Grisel, M Blondel, P Prettenhofer, R Weiss, V Dubourg et al. 2011. “Scikit-learn: Machine Learning in Python.” *Journal of Machine Learning Research* 12(October):2825-2830.

Princeton University Subsurface Hydrology Research Group. n.d. Accessed May 7, 2021. http://co2interface.princeton.edu

Shannon CE and W Weaver. 1949. *The Mathematical Theory of Communication*. University of Illinois Press, Urbana, IL.

Sminchak JR, M Moody, N Gupta, and G Larsen. 2016. “Wellbore integrity factors for CO_2 storage in oil and gas producing areas in the Midwest United States.” *Greenhouse Gases: Science and Technology* 7(October):817-827. https://doi.org/10.1002/ghg.1599

Schlumberger. n.d. Accessed Jun 9, 2021. https://www.software.slb.com/products/eclipse

USEPA. 2010. “Federal Requirements Under the Underground Injection Control (UIC) Program for Carbon Dioxide (CO_2) Geologic Sequestration (GS) Wells.” *Federal Register*, 75 FR 77230, December 10, 2010.

USGS. 2013. *National Assessment of Geologic Carbon Dioxide Storage Resources — Data*. Data Series 774, Version 1.1, U.S. Geological Survey, Geologic Carbon Dioxide Storage Resources Assessment Team, Reston, VA.

White MD, DJ Watson, DH Bacon, SK White, BP McGrail, and ZF Zhang. 2012. *STOMP Subsurface Transport Over Multiple Phases. STOMP-CO2 and -CO2e Guide*. PNNL-21268, Pacific Northwest National Laboratory, Richland, WA.

White S, S Carroll, S Chu, D Bacon, R Pawar, L Cumming, J Hawkins, M Kelley, I Demirkanli, R Middleton et al. 2020. “A risk-based approach to evaluating the Area of Review and leakage risks at CO_2 storage sites.” *International Journal of Greenhouse Gas Control* 93(February):102884. https://doi.org/10.1016/j.ijggc.2019.102884

Yonkofski C. G Tartakovsky, N Huerta, and A Wentworth. 2019. “Risk-based monitoring designs for detecting CO_2 leakage through abandoned wellbores: An application of NRAP’s WLAT and DREAM tools.” *International Journal of Greenhouse Gas Control* 91(December):102807. https://doi.org/10.1016/j.ijggc.2019.102807

Appendix A – References for Geological Parameters

Table A.1. Reference for the ranges of the parameters.

Parameters	Reference
Permeability	Doughty 2009; Birkholzer and Quanlin 2009; Celia et al. 2011; Finley 2014; Akinnikawe et al. 2016; Nguyen et al. 2017; Yonkofski et al. 2019
Porosity	Doughty 2009; Birkholzer et al. 2009; Celia et al. 2011; Finley 2014; Akinnikawe and Ehlig-Economides 2016; Nguyen et al. 2017
Lateral size	Doughty 2009; Celia et al. 2011; Nguyen et al. 2017; Cumming et al. 2019; Sminchak et al. 2016; Onishi et al. 2019
Thickness	Doughty 2009; Celia et al. 2011; Yonkofski et al. 2019; Onishi et al. 2019
Bottom depth	USGS 2013
Temperature gradient	Doughty 2009; Yonkofski et al. 2019
Period	Bacon et al. 2020; White et al. 2020
Total injection amount	Bacon et al. 2020; White et al. 2020

Pacific Northwest National Laboratory

902 Battelle Boulevard
P.O. Box 999
Richland, WA 99354
1-888-375-PNNL (7665)

www.pnnl.gov